ISBN: 978-3-95450-229-5 ISSN: 2673-5520 doi:10.18429/JACoW-MEDSI2020-WEPC07

THERMAL MODEL VALIDATION FOR THE CRYOGENIC MIRROR SYSTEMS FOR SIRIUS/LNLS

L.M. Volpe*, B.A. Francisco†, J.C. Corsaletti, R.R. Geraldes, M. Saveri Silva
Brazilian Synchrotron Light Laboratory (LNLS), Brazilian Center for Research in Energy and Materials
CNPEM, Campinas, São Paulo, Brazil

Abstract

One of the challenges of fourth-generation synchrotron light sources as Sirius at the Brazilian Synchrotron Light Laboratory (LNLS) is the high power density that may affect the beamline optical elements by causing figure deformations that deteriorate the quality of the beam. Indeed, surface specifications for height errors of X-ray mirrors are often within a few nanometers. To deal with these thermal management challenges, thermo-mechanical designs based on cryogenic silicon have been developed, taking advantage of its high thermal conductance and low thermal expansion in temperatures of about 125 K. A liquid nitrogen (LN2) cryostat connected to the optics by copper braids has been used to handle moderate power loads, reducing costs when compared to closed-circuit LN2 cryocoolers and mechanically decoupling flow-induced vibrations from the optics. To guarantee the functionality of such systems, lumped mass thermal models were implemented together with auxiliary finite elements analyses. With the first systems in operation, it has been possible to compare and validate the developed models, and to carry out optimizations to improve them for future projects, by adjusting parameters such as emissivity, thermal contact resistance, and copper braid conductance. This work presents the updated models for CARNAÚBA and CATERETÊ beamlines as reference cases.

INTRODUCTION

The analysis of thermal deformation in synchrotron mirrors is a well known research field due to the impacts in the final shape of the beam [1]. At Sirius, the 4th-generation light source at the Brazilian Synchrotron Light Laboratory (LNLS), this issue has been addressed with an innovative thermo-mechanical concept for exactly-constrained cryocooled mirrors, as detailed in [2]. Indeed, given the high conductivity and the quasi-zero-expansion properties of silicon around 125 K, detrimental thermal effects can be minimized. Here, the methodology and latest developments in thermal models for Sirius mirrors are presented, with the CARNAÚBA and CATERETÊ beamlines taken as study cases due to their demanding requirements concerning small beam sizes and high coherence [3,4]. With lower modeling effort and computational cost for the complex mirror systems, lumped mass models in MATLAB Simscape® have been preferred over finite element analyses (FEA), which are then used mainly as complementary tools as to define control parameters temperature PID, power heater and diagnosis fails in the system.

METHODOLOGY

In lumped mass models, bodies and assemblies in complex geometries can be reduced as nodes with thermal resistances and thermal masses, which are combined according to parameters such as Biot and Fourier number [5]. The example of a node in Simscape is shown in Fig. 1.

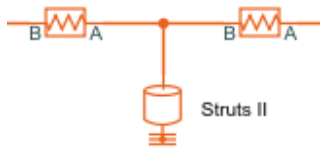

Figure 1: The center block represent the mass of the "struts II" and others are two resistances that represents the conductances between the center of the body and their extremes wich are in contact with other bodies. The central point represent the middle temperature.

Thermal Conduction Resistance

For an 1D solid between two nodes of interest, for example, the conduction thermal resistance may be derived from Fourier's law in Eq. (1), where: Q is the heat flow; ΔT the temperature gradient between the ends of the body; A the cross section; k the thermal conductivity and Δx the solid length. Then, according to Eq. (2), the resistance R is often defined as the inverse of the conductance g, given by the ratio between Q and ΔT. For more complex bodies, the conductances can be calculated after splitting them into simpler bodies or by FEA.

$$Q = \frac{kA\Delta T}{\Delta x} \tag{1}$$

$$g = \frac{Q}{\Delta T} = \frac{kA}{\Delta x} \longrightarrow R = \frac{1}{g} = \frac{\Delta x}{kA} \tag{2}$$

Thermal Contact Resistance

The interfaces between bodies are also modelled as resistances and then associated with the node resistances. As shown in Eq. (3), the contact resistance R_c can be written as a function of the heat flux Q and the temperature difference between surfaces ΔT, being typically extracted from experimental results and/or literature estimates [6,7].

$$Q = \frac{1}{R_c}\Delta T = g_c \Delta T \tag{3}$$

* lucas.volpe@lnls.br
† barbara.francisco@lnls.br

ISBN: 978-3-95450-229-5 ISSN: 2673-5520 doi:10.18429/JACoW-MEDSI2020-WEPC07

Thermal Convection Resistance

The convection heat exchange with fluids can also be modelled using the concept of resistance, being derived from Newton's law in Eq. (4), where: h is the average convection coefficient; A, the contact surface area between the fluid and the solid; T_∞, the temperature of the far fluid; and T_s the surface temperature. As shown in Eq. (5), the convective resistance R_{conv} can be written as a function of the heat flux Q and the temperature difference, being extracted from FEA simulations, experimental results and/or literature.

$$Q = (T_\infty - T_s)\int_A h(A)dA = (T_\infty - T_s)hA \quad (4)$$

$$g_{conv} = \frac{Q}{(T_\infty - T_s)} \longrightarrow R_{conv} = \frac{1}{g_{conv}} \quad (5)$$

Thermal Radiation Resistance

The radiative heat exchange from a body i to a body j can be calculated using Eq. (6), where $\sigma = 5.67\text{x}10^{-8}$ $\text{Wm}^{-2}\text{K}^{-4}$ is the Stefan-Boltzmann constant; T_i and T_j are the temperatures of the bodies; ϵ_i is the emissivity of body i as compared with an ideal blackbody; and B_{ij} is the Gebhart factor, calculated by solving Eq. (7). The view factor F_{ij} is defined "as the part of the radiation emitted by surface i and directly incident on surface j" [5]. The emissivity can be taken from experimental data and/or literature references, whereas the view factors can be conveniently extracted from FEA tools.

$$Q = \epsilon_i A_i B_{ij} \sigma (T_i^4 - T_j^4) \quad (6)$$

$$B_{ij} = F_{ij}\epsilon_j + \Sigma_k F_{ik}(1-\epsilon_k)B_{kj} \quad (7)$$

Another possibility for radiative heat transfer is the net radiation method [8], in which the heat transfer between two bodies is not directly calculated, but the total heat flux among the surfaces can be described.

Lumped Mass Design

Figure 2 shows the steps for a Simscape model. Firstly, a FEA model is implemented in Ansys® assuming constant conductivities and then reproduced in Simscape. After this, upgrades including variable conductivity and radiative heat transfer are included.

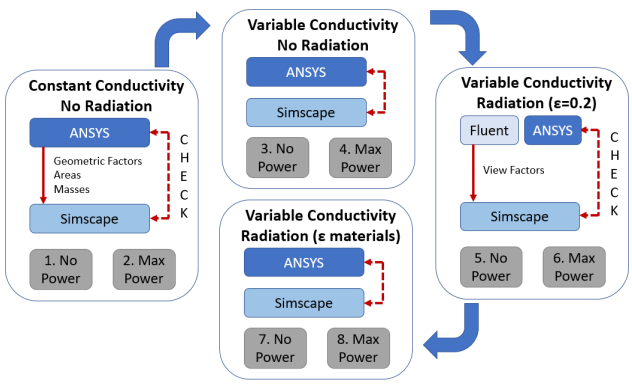

Figure 2: Steps to develop the lumped mass models.

RESULTS

Comparison Between the Models

Figure 3 shows the comparison between Simscape and FEA models for the temperature of the components in the first mirror of CATERETÊ (M1 CAT). The enumerated cases correspond to those in Fig. 2 and the major differences occur when the heat exchange by radiation (cases 5–8) is considered, reaching a maximum of about 17 K in the mirror support.

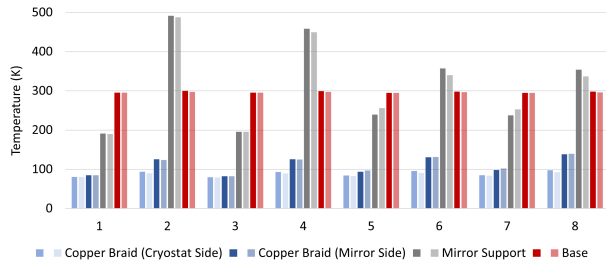

Figure 3: Comparison between FEA (dark) and lumped mass (light) models with temperatures for the CATERETÊ M1 mirror. Numbers in the x-axis are the cases in Fig. 2.

When reviewed the design that we used to FEA simulation, we observed that leaf springs that were in contact with the mirror support presented gradient around 52 K. We modeled these bodies in Simscape as a single part. We suspect that when applied to the radiative heat exchange model, the radiative heat exchanges across the entire piece were not considered, but everything was simplified by considering only the temperatures of the body borders. We will further investigate this question in the development of next models.

Comparison Between the Models and Real Systems

After commissioning the first beamlines, lumped mass models can be compared with the real systems. The first mirrors at CATERETÊ and CARNAÚBA (M1 CAT and M1 CNB) (Fig. 4) are discussed considering their specificities.

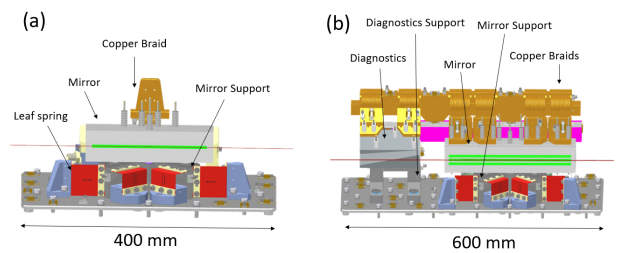

Figure 4: Drawings of Sirius mirror systems: (a) M1 CAT and (b) M1 CNB.

M1 CAT: To create evaluation cases, heat loads were experimentally applied to the mirror and its support frame according to Fig. 5, and also simulated in lumped mass and FEA models.

ISBN: 978-3-95450-229-5 ISSN: 2673-5520 doi:10.18429/JACoW-MEDSI2020-WEPC07

Initially, significant differences were found between experimental and simulated data, and the cause could be eventually associated to the efficiency of the cooling copper braids. As shown in Fig. 6, a better agreement has been achieved by reducing the nominal efficiency by 50%, with closer agreement in the FEA simulations.

The limited performance of the first-generation copper braids made in house led to the developed of a new version, with superior performance [9]. Finally, the major difference between measured and modeled temperatures happens in the mirror support as discussed in the previous section.

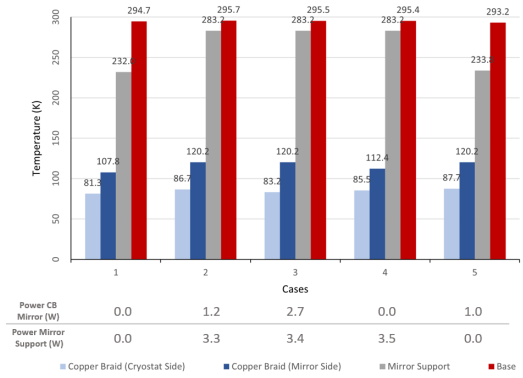

Figure 5: Temperatures in M1 CAT for different power loads.

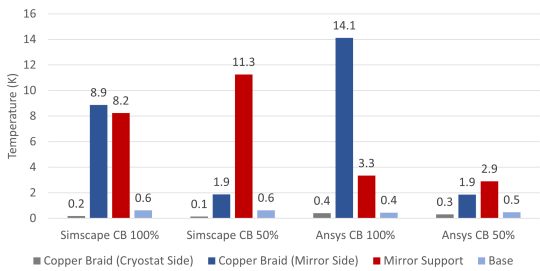

Figure 6: Average of the absolute temperature errors obtained for the five cases presented in Fig. 5 for M1 CAT in comparison with FEA and lumped mass models considering different copper braid efficiencies.

M1 CNB: As in the previous system, different heat loads were applied on the M1 CNB system, as shown in Table 1. Such system is composed of two optics (the mirror M1 and a silicon diagnostic) assembled on independent supports and mounted to a copper rod clamped to two cryostats [10]. In addition, the new-generation braids were already used in this design. The variation of the lumped mass model compared with the measurement is shown in Fig. 7. The divergence found in the mirror support pointed out in Fig. 3 and Fig. 6 was also found here. As previously, each leaf spring had been modelled as a single part, which adds to the hypothesis of they being responsible for the differences.

Other variations observed were the model that we designed to represent both cryostats of this system did not consider the flux variation of the LN2 seen during the operation. The flux variation happens specially during the filling

Table 1: Power (W) Applying in Three Different Measurements in Different Bodies in the M1 of the Carnauba's Beamline

Bodies	Case 1	Case 2	Case 3	Case 4
Diag.	0	0.4	2.9	16.9
Diag. Support	0	0.4	6.9	1.1
M1	0	5.2	10.9	35.8
M1 Support	0	1.5	5.0	3.7

of the liquid nitrogen cylinders that feed the system [11] and are distinct between one cryostat and the other since it is not directly controlled and it is subject to obstruction, level, and pressure fluctuations.

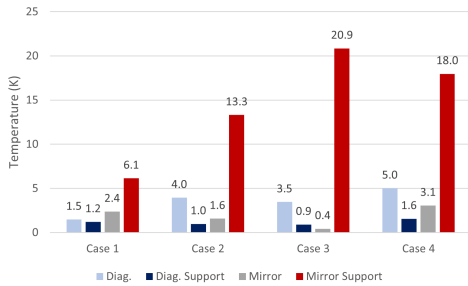

Figure 7: Temperature differences between measurements and simulated by lumped mass model in Simscape.

CONCLUSION

The updated lumped mass models have contributed to validate and improve thermal modeling of the first mirror systems, not only defining power requirements for control heaters and PID control parameters under variable operational conditions. Also diagnosing system issues, as the manufacturing limitations of the first copper braids. Furthermore, a trustful Simscape model makes the dimension of the parts during the design phase faster than by using FEA, since it is necessary only changing numbers instead of redraw pieces.

The differences founded between models and measurements were below 10 K and in the non critics elements. Apart from refinement of model bodies with high gradients (52 K), we are currently optimizing the nitrogen flux system.

Although the mentioned divergences, this modelling technique proves to be enough to the application, keeping the mirror deformation within the requirements and has been also used in other mirrors and monochromator projects on Sirius.

ACKNOWLEDGEMENTS

The authors would like to gratefully acknowledge the funding by the Brazilian Ministry of Science, Technology and Innovation and the contributions of the LNLS team.

ISBN: 978-3-95450-229-5 ISSN: 2673-5520 doi:10.18429/JACoW-MEDSI2020-WEPC07

REFERENCES

[1] Z. Xu *et al.*, "Study on cooling for optical parts with high heat loads at the SSRF", *J. Phys. Conf. Ser.*, vol. 425, no. 5, p. 052011, 2013. doi:10.1088/1742-6596/425/5/052011

[2] R.R. Geraldes *et al.*, "The Design of Exactly-Constrained X-Ray Mirror Systems for Sirius", in *Proc. MEDSI'18*, Paris, France, Jun 2018, pp. 173–178. doi:10.18429/JACoW-MEDSI2018-WEOAMA04

[3] H. C. N. Tolentino *et al.*, "Innovative instruments based on cryogenically cooled silicon crystals for the CARNAÚBA beamline at Sirius-LNLS", *AIP Conference Proceedings*, vol. 2054, p. 060026, 2019. doi:10.1063/1.5084657

[4] F. Meneau *et al.*, "Cateretê, the Coherent Scattering Beamline at Sirius, 4th Generation Brazilian Synchrotron Facility", presented at Workshop on Coherence at ESRF-EBS, Grenoble, France, 2019.

[5] Dutch Society for Precision Engineering (DSPE), https://www.dspe.nl/knowledge/thermomechanics/chapter-2-in-depth/2-4-thermal-radiation/2-4-3-gebhard-method/

[6] S. Scott, "Thermal contact between Silicon and Copper", MEDSI Design Guidelines, pp. 1-4, 2016. https://medsi.lbl.gov/files/page_159/Thermal_contact_between_silicon_and_copper.doc

[7] F.P. Incropera *et al.*, *Fundamentals of Heat and Mass Transfer*, 7. ed. Hoboken, NJ: John Wiley, 2011.

[8] J. H. Lienhard IV and J. H. Lienhard V, *A Heat Transfer Textbook*. 4th. ed. Cambridge, MA, USA: Phlogiston Press, 2018.

[9] F.R. Lena *et al.*, "Copper braid heat conductors for Sirius Cryogenic X-ray Optics", presented at MEDSI'20, Chicago, USA, Jul 2021, paper TUPC14, this conference.

[10] H. C. N. Tolentino *et al.*, "X-ray microscopy developments at Sirius-LNLS: first commissioning experiments at the Carnauba beamline", *Proc. SPIE 11839, X-Ray Nanoimaging: Instruments and Methods V*, p. 83904, Aug. 2021. doi:10.1117/12.2596496

[11] M. Saveri Silva *et al.*, "Cryogenic Systems for Optical Elements Cooling at Sirius/LNLS", presented at MEDSI'20, Chicago, USA, Jul 2021, paper MOPB02, this conference.